SLAC-PUB-16209

Enhanced Electrical Transparency by Ultra-Thin $LaAlO_3$ Insertion at Oxide Metal/Semiconductor Heterointerfaces

Takeaki Yajima,[†,‡] Makoto Minohara,[†,§,∥] Christopher Bell,[†,¶] Hiroshi Kumigashira,[∥] Masaharu Oshima,[#] Harold Y. Hwang,[†,§] and Yasuyuki Hikita*[†]*

[†]Stanford Institute for Materials and Energy Sciences, SLAC National Accelerator Laboratory, Menlo Park, California 94025, USA

[‡]Department of Materials Engineering, The University of Tokyo, Bunkyo, Tokyo 277-8561, Japan

[§]Geballe Laboratory for Advanced Materials, Department of Applied Physics, Stanford University, Stanford, California 94305, USA

[∥] Photon Factory, High Energy Accelerator Research Organization, Tsukuba, Ibaraki 305-0801, Japan

[#]Department of Applied Chemistry, The University of Tokyo, Bunkyo, Tokyo 113-8656, Japan

This material is based upon work supported by the U.S. Department of Energy, Office of Science, Office of Basic Energy Sciences, under Contract No. DE-AC02-76SF00515 and LDRD.

We demonstrate that the electrical conductivity of metal/semiconductor oxide heterojunctions can be increased over seven orders of magnitude by inserting an ultra-thin layer of $LaAlO_3$. This counterintuitive result, that an interfacial barrier can be driven transparent by inserting a wide-gap insulator, arises from large internal electric field between the two polar $LaAlO_3$ surfaces. This field modifies the effective band offset in the device, highlighting the ability to design the electrostatic boundary conditions with atomic precision.

KEYWORDS: Interface dipole, Polar discontinuity, Schottky junction, Perovskite oxide, $LaAlO_3$

Interfaces and surfaces show a rich variety of emergent physical phenomena, ranging from confined electronic phases in strongly correlated electronic systems,[1-4] to catalytic behaviors.[5-7] To fully exploit these phenomena in devices, atomic scale control is indispensable. For example, the contact resistance in silicon devices can be reduced using interface dipoles,[8] and the development of advanced catalysts requires precise tuning of the surface molecular reactions.[9,10] Manipulation of the interface or surface band diagram, which defines the electronic properties of these devices, can be achieved via charges originated from dopant ions,[11] interface states,[12] ferroelectric polarization,[13-16] surface adsorbates,[17] and so on, which can electrostatically modify the electron energies nearby. This approach is especially effective in ionic materials, where a high concentration of charges can be simply manipulated via the positioning of the ions. By controlling the ionic stacking sequence, charges can be embedded on the atomic scale, creating clean low-dimensional electronic systems,[18,19] as well as combining distinctive electronic phases to create unique interfacial states.[3,4]

These considerations are particularly relevant to the recent development of atomic-scale perovskite oxide heterostructures, which has created a wealth of new opportunities via the integration of their rich variety of physical properties, and enabled by their inherently small lattice mismatch. In particular, interfacial phenomena distinct from the bulk can be engineered, such as electrical conductivity between insulators,[1,2] interface superconductivity,[3] and ferromagnetism between antiferromagnets.[4] While these striking properties are often manifested through in-plane transport measurements, here we demonstrate a highly interfacial phenomenon which controls the out-of-plane transport properties. The electrical conductivity of $SrRuO_3$/Nb:$SrTiO_3$ {100} metal/semiconductor Schottky junctions can be tuned over seven orders of magnitude by inserting a wide-gap (5.6 eV) insulator $LaAlO_3$, with thicknesses from 0 to 3 unit cells (uc). Electrical measurements and photoemission spectroscopy (PES) show that a large internal electric field exists on the angstrom-scale, modifying the effective band offset at the heterointerface. This electric field is attributed to the ionic $(LaO)^+$ and $(AlO_2)^-$ sheet charges in the $LaAlO_3$ interlayer.

The Schottky barrier height (SBH), a key parameter of these junctions, is given by the difference between the metal work function and the semiconductor electron affinity. When an interface dipole of magnitude Δ exists at the junction, the SBH is shifted up or down by Δ. Thus a measurement of the SBH provides an excellent measure for the dipole potential introduced by the $LaAlO_3$ insertion. Here the SBH was measured by current-voltage (*I*-*V*), capacitance-voltage (*C*-*V*), and PES measurements.

Figure 1a,b shows the *I*–*V* characteristics of the various $SrRuO_3$/$LaAlO_3$/Nb:$SrTiO_3$ Schottky junctions, in a linear and a semi-logarithmic plot. Qualitatively, it is clear that inserting $LaAlO_3$ continuously decreases the asymmetry of the rectifying *I*–*V* curves, finally producing an Ohmic

junction with 2 uc of $LaAlO_3$. The linear relationship between log(I) and V was obtained for all rectifying junctions under forward bias, representing ideal thermionic emission characteristics[20] with ideality factors < 1.1 even with the $LaAlO_3$ interlayers. The insertion of an insulator enhances the current from < 10^{-9} A to 10^{-2} A at a bias voltage of -1 V, a change of more than seven orders of magnitude, drastically affecting the device properties, as shown schematically in Figures 1c and d.

Quantitatively the SBH can be evaluated from the I-V measurements, using the thermionic emission model,[20] which accurately describes the log(I)-V linear curves. The calculated SBH, extracted from an extrapolated linear fit in the forward bias region, proportionally decreased with $LaAlO_3$ insertion, indicating an increase in Δ. In the C-V characteristics, $1/C^2$ was a linear function of V in accordance with the Mott-Schottky model[20] (Figure 2a). The built-in potential in Nb:$SrTiO_3$ was deduced from the abscissa intercept of the linear extrapolation, which decreased consistently with the I-V analysis. Here the built-in potential is approximately 0.1 eV smaller than the SBH for the doping concentration employed.

Using PES, we measured the binding energy (E_b) of the Ti $2p_{3/2}$ core level in the vicinity of the junctions, with respect to E_F of the whole system. The shift in E_b indicates a change in the electrostatic potential of the interfacial Ti atoms with respect to the grounded metallic layer, *i.e.* a change in the band bending, and hence the SBH. Here the Ti $2p_{3/2}$ spectra are shifted to higher binding energies, indicating a decrease in the SBH by $LaAlO_3$ insertion (Figure 2b). The measured SBHs from all of the three different measurements, summarized in Figure 2c, clearly show a collapse of the SBH due to the formation of an interface dipole by the inserted $LaAlO_3$.

This interface dipole can be understood by considering the ionic layers within the $LaAlO_3$ crystal in the pseudo-cubic {100} directions (Figure 3a). Here, we regard the perovskite structure

(ABO_3) as stacking planes of AO and BO_2, which in $LaAlO_3$ are $(LaO)^+$ and $(AlO_2)^-$, in contrast with the neutral layers of both $SrTiO_3$: $(SrO)^0$ and $(TiO_2)^0$, and $SrRuO_3$: $(SrO)^0$ and $(RuO_2)^0$ in a simple ionic picture. Because the $(LaO)^+$ and $(AlO_2)^-$planes are displaced by 0.5 uc in $LaAlO_3$, an electrostatic potential from the dipole moment Δ forms. Then, this electrostatic potential shifts the SBH, as visualized by the change of the band diagram from Figure 3b (without $LaAlO_3$ insertion) to Figure 3c (with $LaAlO_3$ insertion).

Notably, the effect of the ionic layers in $LaAlO_3$ has been actively discussed in the context of the $LaAlO_3/SrTiO_3$ {100} heterointerface, where a high mobility electron gas is accumulated at the interface[1]. The relative contributions to the electronic accumulation from interfacial oxygen vacancies,[21,22] La interdiffusion into $SrTiO_3$,[23,24] and an electronic reconstruction[25] to solve the polarity mismatch between the $(LaO)^+$ - $(AlO_2)^-$, and the $(SrO)^0$ - $(TiO_2)^0$ layers[26] have been discussed. Strikingly, conducting electrons exist only above some critical $LaAlO_3$ thickness, between 3 and 4 uc,[27] while below 3 uc, it is predicted that a build-up of an internal electric field in the $LaAlO_3$ is more energetically favored.[23,28,29] However, the values of this internal electric field that have been measured, or inferred to exist, in the $LaAlO_3$ have widely varied among different experiments using various techniques.

For example, PES revealed a significant reduction of the internal electric field from the predicted value.[30,31] Transport studies have hinted at this field's influence,[32] however evidence of extreme sensitivity to surface adsorbates[17] suggests that the surface electrostatic boundary conditions can be strongly modified, depending on the details of the sample preparation[17] or surface reconstructions.[33] A critical difference of our study from previous ones[30,31] is that an ideally wetting, epitaxial, $SrRuO_3$ metallic layer caps the $LaAlO_3$ surface, unambiguously defining the boundary conditions of the band diagram as predicted by theoretical

calculations.[34,35] Furthermore, the large work function of $SrRuO_3$ depletes the electrons in the Nb:$SrTiO_3$ close to the interface at the $LaAlO_3$ thickness of 1 uc where Δ is still below the original SBH ~ 1.3 eV. This depletion regime prohibits electron accumulation at the $LaAlO_3$/Nb:$SrTiO_3$ {100} interface, preserving the maximum internal electric field in the $LaAlO_3$ interlayer.

To further confirm the absence/existence of the internal electric field in the $LaAlO_3$ layer, PES was performed on $SrRuO_3$/$LaAlO_3$/Nb:$SrTiO_3$ heterostructures, as well as for uncapped $LaAlO_3$/Nb:$SrTiO_3$ samples. In Figure 4a, Al 2*p* core level spectra are plotted with respect to Ti $2p_{3/2}$ core level energy. Here 800 eV X-rays at relatively high output angle were used to achieve short photoelectron escape depths ~ 1 uc (see Methods Section), enabling the detection of only the topmost atomic layers for a given atomic species. The shift of the peaks (shown with the red arrows) indicates that the electrostatic potential between the topmost Al in $LaAlO_3$ and the topmost Ti in Nb:$SrTiO_3$ was shifted by the $SrRuO_3$ capping. Similar results were obtained from the analysis of Al 2*p* core levels with respect to La $4d_{3/2}$ core levels (Figure 4b), where the 0.5 uc difference between the positions of the topmost Al and La atoms in $LaAlO_3$ (Figure 3a) was exploited to confirm the internal electric field in the $LaAlO_3$ interlayers. In both spectra, the topmost Al atoms are closer to the surface than the topmost Ti or La atoms (Figure 3a), and the increase in the Al 2*p* core level energies with respect to Ti $2p_{3/2}$ or La $4d_{3/2}$ corresponds to an increased electron energy on the surface side of the $LaAlO_3$. The estimated internal electric field ~ 1 eV/uc and the resulting relative dielectric constant ~24 (almost identical to the $LaAlO_3$ bulk value[36]) are consistent with the previous estimates based on the first principle calculations.[23,28,29]

We note that the shift of the PES peak position as a function of $LaAlO_3$ thickness tends to saturate between 1 and 2 uc, somewhat below the critical thickness observed in the uncapped

$LaAlO_3/SrTiO_3$ system. This difference is physically very reasonable, and a natural consequence of the different energy thresholds in the two systems – the Schottky junctions being defined by the original SBH ~ 1.3 eV, in contrast to the 3.2 eV $SrTiO_3$ band-gap in the $LaAlO_3/SrTiO_3$ case. In the Schottky junctions, the ~ 1.3 eV scale, fixed by the $SrRuO_3/Nb:SrTiO_3$ band offset, corresponds to a transition where the $LaAlO_3/Nb:SrTiO_3$ interface switches from depletion to accumulation modes. This transition can be visually understood in the band diagrams in Figure 3b,c. The increase in the $LaAlO_3$ thickness weakens the depletion in $Nb:SrTiO_3$ as indicated by the red arrows in Figure 3c, and the further increase in thickness totally suppresses the depletion and induces an accumulation of electrons at the $LaAlO_3/Nb:SrTiO_3$ interface instead. Crucially, these PES shifts are consistent with the observed interface dipoles in Figures 1 and 2, confirming our interpretation above using an idealized model. It should also be noted that the 2 uc $LaAlO_3$ insertion lead to the Ohmic behavior (Figure 1a) although the tunneling barrier of $LaAlO_3$ still remains after the collapse of the SBH. This is because the tunneling barrier of the 2 uc $LaAlO_3$ layer is much less resistive than the other series resistance of the whole circuit ~100 Ω, resulting in the Ohmic behavior which only reflects this series resistance.

In summary, we have demonstrated that an epitaxial Schottky barrier can be driven Ohmic by the insertion of a wide-gap insulator with polar surfaces. In addition to providing a flexible method for widely tuning band alignments in oxide heterostructures, this can be used to impart large internal electric fields across thin film components, which have been theoretically proposed for novel photovoltaic devices.[37]

Methods. The Schottky junctions were formed between a metallic single crystalline $SrRuO_3$ film and an *n*-type semiconducting Nb-doped (0.01 wt. %) $SrTiO_3$ {100} substrate. Both materials have a common perovskite structure with small lattice mismatch of ~0.5 %, facilitating

epitaxial Schottky junctions with ideal characteristics.[38,39] The $SrRuO_3$ and $LaAlO_3$ were grown by pulsed laser deposition using TiO_2-terminated Nb:$SrTiO_3$ {100} substrates. $LaAlO_3$ was grown in an O_2 partial pressure of 1×10^{-5} Torr, while $SrRuO_3$ (60 uc for electrical measurements and 5 ~ 6 uc for PES) was grown at 0.3 Torr. The substrate temperature was 750 ^oC in all cases. The samples were *ex situ* post-annealed in 760 Torr O_2 at 350 ^oC for 6 hours to fill possible oxygen vacancies. For Ohmic contacts, gold was evaporated onto the $SrRuO_3$ and indium was ultrasonically soldered onto the Nb:$SrTiO_3$. The PES measurements using synchrotron radiation were carried out on beamline BL2C at the Photon Factory in KEK, Japan, with 800 eV incident photon energy. The PES spectra were recorded using a Scienta SES-2002 electron energy analyzer with a total energy resolution of 150 meV. For the PES experiments, 5 ~ 6 uc thick $SrRuO_3$ films were used to minimize the attenuation of the emitted photoelectrons. The detection angle was set to 60^o for $SrRuO_3/LaAlO_3$/Nb:$SrTiO_3$ samples and 80^o for $LaAlO_3$/Nb:$SrTiO_3$ samples, such that the PES signal was sensitive to only the topmost atomic planes for a given atomic species.

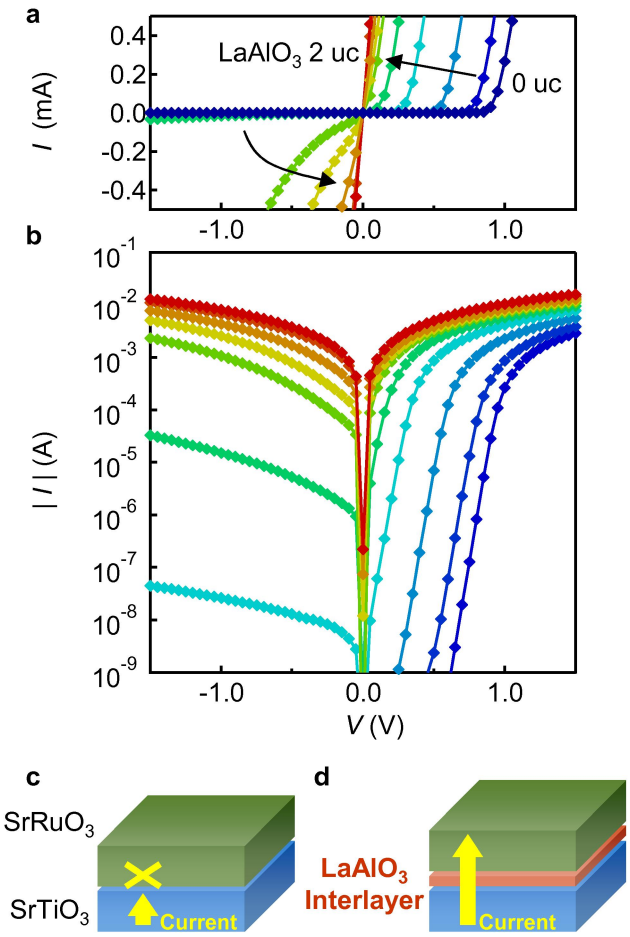

Figure 1. *I-V* characteristics of $SrRuO_3/LaAlO_3$ (0 ~ 2 uc)/Nb:$SrTiO_3$ Schottky junctions at room temperature using (a) linear and (b) semi-logarithmic scales. The amount of inserted $LaAlO_3$ is 0, 0.12, 0.36, 0.60, 0.84, 1.1, 1.3, 1.6, 1.8, 2.0 uc from blue to red. Schematic illustrations of vertical current flow under reverse bias (c) without and (d) with $LaAlO_3$ insertion.

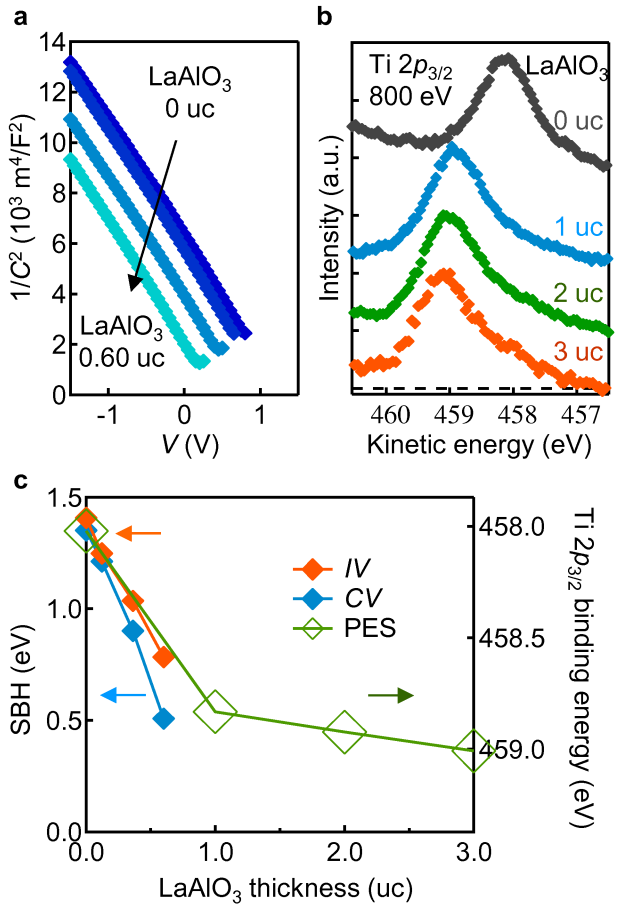

Figure 2. Schottky barrier height measurements. (a) *C*-*V* characteristics ($LaAlO_3$ thickness 0, 0.12, 0.36, 0.60 uc from top to bottom) and (b) Ti $2p_{3/2}$ photoemission spectra of $SrRuO_3/LaAlO_3/Nb:SrTiO_3$ Schottky junctions at room temperature for various $LaAlO_3$ thicknesses. (c) Summary of SBHs and Ti $2p_{3/2}$ binding energy as a function of $LaAlO_3$ thickness.

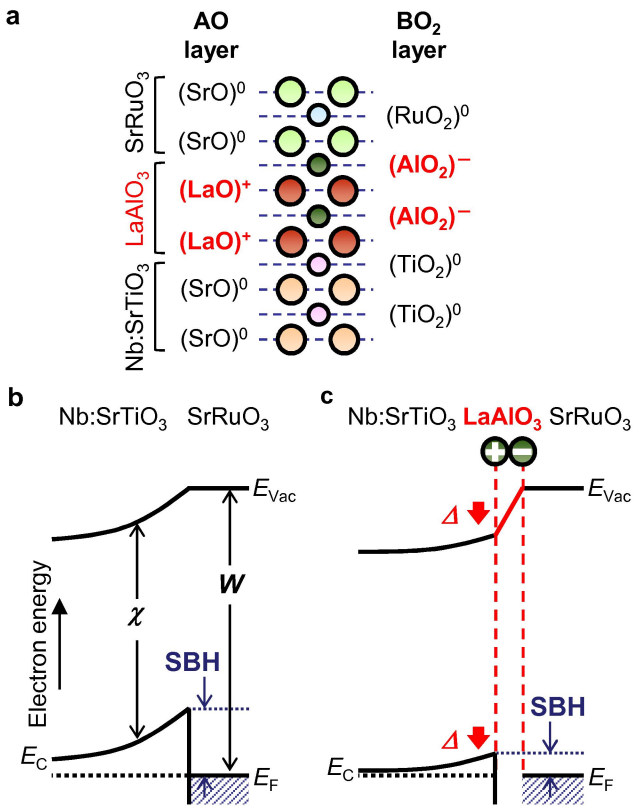

Figure 3. Interface dipole of the $LaAlO_3$ layer. (a) Schematic illustrations of the ionic layer sequences (anions not shown) at a $SrRuO_3/LaAlO_3/Nb:SrTiO_3$ Schottky junction. (b,c) The band diagrams of $SrRuO_3/Nb:SrTiO_3$ Schottky junctions (b) without and (c) with $LaAlO_3$ insertion. E_{Vac}, E_C, and E_F are the vacuum level, the conduction band edge, and the Fermi level respectively. In (b), χ and W represent the electron affinity of $Nb:SrTiO_3$ and the work function of $SrRuO_3$. In (c), the solid red line indicates the dipole potential of the $LaAlO_3$ layer, and the red arrows indicate the electrostatic potential shift introduced by this interface dipole.

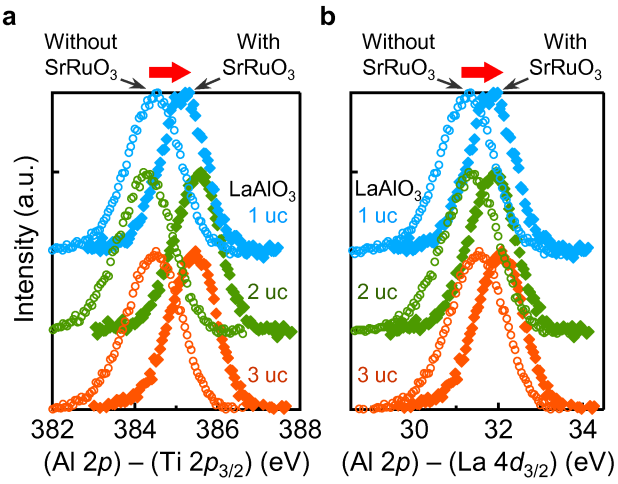

Figure 4. Internal electric field in the $LaAlO_3$ layer via PES. Al 2*p* core level spectra in $SrRuO_3/LaAlO_3/Nb:SrTiO_3$ (solid diamonds) and the $LaAlO_3/Nb:SrTiO_3$ (open circles) heterostructures, for several $LaAlO_3$ thicknesses, plotted with respect to (a) the Ti $2p_{3/2}$ and (b) the La $4d_{3/2}$ core level peak energies. The red arrows indicate the peak energy shift by the $SrRuO_3$ capping.

AUTHOR INFORMATION

Corresponding Author

*E-mail: yajima@adam.t.u-tokyo.ac.jp

*E-mail: hikita@stanford.edu

Present Addresses

¶Current Address: H. H. Wills Physics Laboratory, University of Bristol, Tyndall Avenue, Bristol, BS8 1TL, UK.

Notes

The authors declare no competing financial interest.

ACKNOWLEDGMENT

We acknowledge support from the Department of Energy, Office of Basic Energy Sciences, Division of Materials Sciences and Engineering, under contract DE‐AC02‐76SF00515 (T.Y., Y.H., M.M., C.B., & H.Y.H.). T.Y. also acknowledges support from the Japan Society for the Promotion of Science (JSPS).

REFERENCES

(1) Ohtomo, A.; Hwang, H. Y. *Nature* **2004**, 427, 423-426.

(2) Reyren, N.; Thiel, S.; Caviglia, A. D.; Fitting Kourkoutis, L.; Hammerl, G.; Richter, C.; Schneider, C. W.; Kopp, T.; Rüetschi, A.-S.; Jaccard, D.; Gabay, M.; Muller, D. A.; Triscone, J.-M.; Mannhart, J. *Science* **2007**, 317, 1196-1199.

(3) Gozar, A.; Logvenov, G.; Fitting Kourkoutis, L.; Bollinger, A. T.; Giannuzzi, L. A.; Muller, D. A.; Bozovic, I. *Nature* **2008**, 455, 782-785.

(4) Smadici, S.; Abbamonte, P.; Bhattacharya, A.; Zhai, X.; Jiang, B.; Rusydi, A.; Eckstein, J. N.; Bader, S. D.; Zuo, J.-M. *Phys. Rev. Lett.* **2007**, 99, 196404.

(5) Fujishima, A.; Honda, K. *Nature* **1972**, 238, 37-38.

(6) Grätzel, M. *Nature* **2001**, 414, 338-344.

(7) Kato, H.; Asakura, K.; Kudo, A. *J. Am. Chem. Soc.* **2003**, 125, 3082-3089.

(8) Alshareef, H. N.; Quevedo-Lopez, M. A.; Majhi, P. *MRS Bulletin* **2011**, 36, 90-94.

(9) He, Y.; Tilocca, A.; Dulub, O.; Selloni, A.; Diebold, U. *Nature Mater.* **2009**, 8, 585-589.

(10) Li, S.-C.; Chu, L.-N.; Gong, X.-Q.; Diebold, U. *Science* **2010**, 328, 882-884.

(11) Shannon, J. M. *Solid-State Electron.* **1976**, 19, 537-543.

(12) Bardeen, J. *Phys. Rev.* **1947**, 71, 717-727.

(13) Blom, P. W. M.; Wolf, R. M.; Cillesen, J. F. M.; Krijn, M. P. C. M. *Phys. Rev. Lett.* **1994**, 73, 2107-2110.

(14) Ji, W.; Yao, K.; Liang, Y. C. *Adv. Mater.* **2010**, 22, 1763-1766.

(15) Kim, T. H.; Jeon, B. C.; Min, T.; Yang, S. M.; Lee, D.; Kim, Y. S.; Baek, S.-H.; Saenrang, W.; Eom, C.-B.; Song, T. K.; Yoon, J.-G.; Noh, T. W. *Adv. Funct. Mater.* **2012**, 22, 4962-4968.

(16) Liu, X.; Wang, Y.; Burton, J. D.; Tsymbal, E. Y. *Phys. Rev. B* **2013**, 88, 165139.

(17) Xie, Y. W.; Hikita, Y.; Bell, C.; Hwang, H. Y. *Nature Commun.* **2011**, 2, 494.

(18) Jang, H. W.; Felker, D. A.; Bark, C. W.; Wang, Y.; Niranjan, M. K.; Nelson, C. T.; Zhang, Y.; Su, D.; Folkman, C. M.; Baek, S. H.; Lee, S.; Janicka, K.; Zhu, Y.; Pan, X. Q.; Fong, D. D.; Tsymbal, E. Y.; Rzchowski, M. S.; Eom, C. B. *Science* **2011**, 331, 886-889.

(19) Ohtsuka, R.; Matvejeff, M.; Nishio, K.; Takahashi, R.; Lippmaa, M. *Appl. Phys. Lett.* **2010**, 96, 192111.

(20) Sze, S. M.; Ng, K. K., *Physics of semiconductor devices*, 3rd ed.; John Wiley & Sons: Hoboken, NJ, 2007.

(21) Siemons, W.; Koster, G.; Yamamoto, H.; Harrison, W. A.; Lucovsky, G.; Geballe, T. H.; Blank, D. H. A.; Beasley, M. R. *Phys. Rev. Lett.* **2007**, 98, 196802.

(22) Basletic, M.; Maurice, J.-L.; Carrétéro, C; Herranz, G.; Copie, O.; Bibes, M.; Jacquet, É.; Bouzehouane, K.; Fusil, S.; Barthélémy, A. *Nature Mater*. **2008**, 7, 621-625.

(23) Willmott, P. R.; Pauli, S. A.; Herger, R.; Schlepütz, C. M.; Martoccia, D.; Patterson, B. D.; Delley, B.; Clarke, R.; Kumah, D.; Cionca, C.; Yacoby, Y. *Phys. Rev. Lett.* **2007**, 99, 155502.

(24) Qiao, L.; Droubay, T. C.; Varga, T.; Bowden, M. E.; Shutthanandan, V.; Zhu, Z.; Kaspar, T. C.; Chambers, S. A. *Phys. Rev. B* **2011**, 83, 085408.

(25) Harrison, W. A.; Kraut, E. A.; Waldrop, J. R.; Grant, R. W. *Phys. Rev. B* **1978**, 18, 4402.

(26) Nakagawa, N.; Hwang, H. Y.; Muller, D. A. *Nature Mater*. **2006**, 5, 204-209.

(27) Thiel, S.; Hammerl, G.; Schmehl, A.; Schneider, C. W.; Mannhart, J. *Science* **2006**, 313, 1942-1945.

(28) Lee, J.; Demkov, A. A. *Phys. Rev. B* **2008**, 78, 193104.

(29) Son, W.-J.; Cho, E.; Lee, B.; Lee, J.; Han, S. *Phys. Rev. B* **2009**, 79, 245411.

(30) Segal, Y.; Ngai, J. H.; Reiner, J. W.; Walker, F. J.; Ahn, C. H. *Phys. Rev. B* **2009**, 80, 241107.

(31) Takizawa, M.; Tsuda, S.; Susaki, T.; Hwang, H. Y.; Fujimori, A. *Phys. Rev. B* **2011**, 84, 245124.

(32) Singh-Bhalla, G.; Bell, C.; Ravichandran, J.; Siemons, W.; Hikita, Y.; Salahuddin, S.; Hebard, A. F.; Hwang, H. Y.; Ramesh, R. *Nature Phys.* **2011**, 7, 80-86.

(33) Lanier, C. H.; Rondinelli, J. M.; Deng, B.; Kilaas, R.; Poeppelmeier, K. R.; Marks, L. D. *Phys. Rev. Lett.* **2007**, 98, 086102.

(34) Cazorla, C.; Stengel, M. *Phys. Rev. B* **2012**, 85, 075426.

(35) Arras, R.; Ruiz, V. G.; Pickett, W. E.; Pentcheva, R. *Phys. Rev. B* **2012**, 85, 125404.

(36) Konaka, T.; Sato, M.; Asano, H.; Kubo, S. *J. Superconduct*. **1991**, 4, 283-288.

(37) Assmann, E.; Blaha, P.; Laskowski, R.; Held, K.; Okamoto, S.; Sangiovanni, G. *Phys. Rev. Lett.* **2013**, 110, 078701.

(38) Hikita, Y.; Kozuka, Y.; Susaki, T.; Takagi, H.; Hwang, H. Y. *Appl. Phys. Lett.* **2007**, 90, 143507.

(39) Minohara, M.; Ohkubo, I.; Kumigashira, H.; Oshima, M. *Appl. Phys. Lett.* **2007**, 90, 132123.